Stanford Exploration Project, Report 120, May 3, 2005, pages 285–299

Converted-mode angle-domain common-image gathers for migration velocity analysis

Daniel A. Rosales and Biondo Biondi[1]

ABSTRACT

Common-image gathers are very useful for velocity and petrophysical analysis. Wavefield-extrapolation methods produce Angle-Domain Common-Image Gathers (ADCIGs). For the conventional PP case, ADCIGs are a function of the opening angle. The representation of ADCIGs for PS data (PS-ADCIGs) is more elaborate than for conventional ADCIGs. In PS-ADCIGs, the P-to-S velocity ratio is a major variable in transforming the subsurface offset to the opening angle, and in transforming this opening angle to either the P-incidence or the S-reflection angle. Numerical studies show that when the P-to-S velocity ratio and image midpoint information are not incorporated the error in computing PS-ADCIGs is enough to introduce artifacts in the velocity model.

INTRODUCTION

Imaging is the combined process of migration and velocity analysis. The final image provides two important pieces of information about the subsurface: its structure and some of its rock properties. To obtain a reliable image, we need a reliable velocity model. Therefore, the image process becomes a combined procedure between migration and migration velocity analysis.

The final image by itself provides information about the accuracy of the velocity model. This information is present in the redundancy of the seismic data, that is in non-zero-offset images. The information is distributed along a 3-dimensional image space, for 2D seismic data; the coordinates of this space are $I(z_\xi, m_\xi, h)$. The subsets of this image for a fixed image point (m_ξ) with coordinates (z_ξ, h) are known as common-image gathers (CIG), or common-reflection-point gathers (CRP). If the CIGs are a function of (z_ξ, h), the gathers are also referred to offset-domain common-image gathers (ODCIG). These gathers can also be expressed in terms of an opening angle γ, by transforming the offset axis (h) into the opening angle (γ) to obtain a common image gather with coordinates (z_ξ, γ); these gathers are known as Angle-Domain Common-Image Gathers (ADCIG) (de Bruin et al., 1990; Prucha et al., 1999; Brandsberg-Dahl et al., 1999; Rickett and Sava, 2002; Sava and Fomel, 2003; Biondi and Symes, 2004).

[1]**email:** daniel@sep.stanford.edu, biondo@sep.stanford.edu

There are two kinds of ODCIGs: those produced by Kirchhoff migration, and those produced by wavefield-extrapolation migration, referred to from now on as wave-equation migration. There is a conceptual difference in the offset dimension between these two kinds of gathers. For Kirchhoff ODCIGs, the offset is a data parameter ($h = h_D$), and involves the concept of flat gathers. For wave-equation ODCIGs, the offset dimension is a model parameter ($h = h_\xi$), and involves the concept of focused events. In this paper, we will refer to these gathers as subsurface offset-domain common-image gathers (SODCIG).

There are problems observed with ODCIGs, which can be alleviated by parameterizing the offset axis into an angle axis to form angle-domain common image-gathers. Unlike ODCIGs, ADCIGs produced with either method have similar characteristics, since they describe the reflectivity as a function of the angle at the reflector.

Depending on the seismic experiment we are analyzing, the coordinates of the image space possess different information relevant to the experiment. We refer to a conventional seismic reflection experiment, where the source and the receiver have the same type of wave, as *single-mode* case. The transformation from ODCIGs to ADCIGs is a well-known process in the literature, and in this case the angle axis represents the true reflection angle.

A seismic experiment where the source and the receiver process different types of waves is known as multi-component seismic, throughout this paper, we refer to this experiment as *converted-mode* case, as for example the conversion from P wave into an S wave at the reflection point. This paper discusses the common-image gathers for this kind of experiment, focusing mainly on SODCIGs and their accurate transformation into ADCIGs. We validate our results by generalizing the concepts of Kirchhoff migration.

A final side product of our analysis is the ability to separate the final image into two parts, each one corresponding to a distinctive wave. Throughout this process, the velocity ratio between the different velocities plays an important role in the transformation. We present and analyze the kinematics of our equations and present some synthetic results.

KINEMATIC EQUATIONS

This section describes the kinematic equation that transforms a subsurface offset-domain CIG to an opening-angle-domain CIG, for the converted-mode case. The derivation follows the well-known equations for apparent slowness in a constant-velocity medium in the neighborhood of the reflection/conversion point. Our derivation is consistent with those presented by Fomel (1996);Sava and Fomel (2000); and Biondi (2005).

The expressions for the partial derivatives of the total traveltime with respect to the image

point coordinates are as follows (Rosales and Rickett, 2001a):

$$\begin{aligned}
\frac{\partial t}{\partial m_\xi} &= S_s \sin\beta_s + S_r \sin\beta_r, \\
\frac{\partial t}{\partial h_\xi} &= -S_s \sin\beta_s + S_r \sin\beta_r, \\
-\frac{\partial t}{\partial z_\xi} &= S_s \cos\beta_s + S_r \cos\beta_r.
\end{aligned} \tag{1}$$

Where S_s and S_r are the slowness (inverse of velocity) at the source and receiver locations. Figure 1 illustrates all the angles in this discussion. The angle β_s is the direction of the wave propagation for the source, and the angle β_r is the direction of the wave propagation for the receiver. Through these set of equations, we obtain:

$$\begin{aligned}
-\frac{\partial z_\xi}{\partial h_\xi} &= \frac{S_r \sin\beta_r - S_s \sin\beta_s}{S_r \cos\beta_r + S_s \cos\beta_s}, \\
-\frac{\partial z_\xi}{\partial m_\xi} &= \frac{S_s \sin\beta_s + S_r \sin\beta_r}{S_s \cos\beta_s + S_r \cos\beta_r}.
\end{aligned} \tag{2}$$

We define two angles, α and γ, to relate β_s and β_r as follows:

$$\alpha = \frac{\beta_r + \beta_s}{2}, \quad \text{and} \quad \gamma = \frac{\beta_r - \beta_s}{2}. \tag{3}$$

The meaning of the angles α and γ will become clear later in the paper; for now, we will refer to γ as the *full-aperture* angle. Through the change of angles presented on equation (3), and by following basic trigonometric identities, we can rewrite equations (2) as follows:

$$\begin{aligned}
-\frac{\partial z_\xi}{\partial h_\xi} &= \frac{\tan\gamma + \mathcal{S}\tan\alpha}{1 - \mathcal{S}\tan\alpha\tan\gamma}, \\
-\frac{\partial z_\xi}{\partial m_\xi} &= \frac{\tan\alpha + \mathcal{S}\tan\gamma}{1 - \mathcal{S}\tan\gamma\tan\alpha}
\end{aligned} \tag{4}$$

where,

$$\mathcal{S} = \frac{S_r - S_s}{S_r + S_s} = \frac{\phi - 1}{\phi + 1}, \tag{5}$$

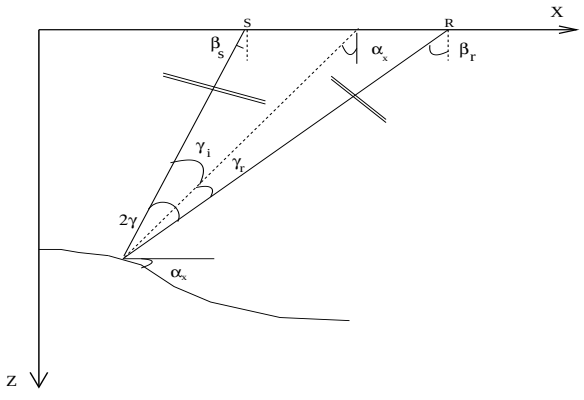

Figure 1: Angle definition for the kinematic equation of converted mode ADCIGs daniel2-angles [NR]

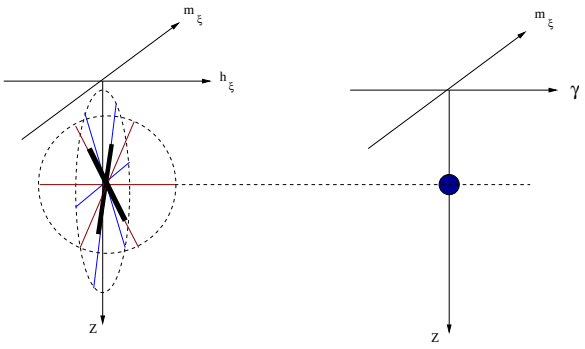

Figure 2: Slant stack angle transformation from SODCIGs to ADCIGs. This transformation allows lateral and vertical variation of $\mathcal{S}$. daniel2-sketch [NR]

and ϕ is the velocity ratio, as for example the P-to-S velocity ratio. This leads to quadratic equations for $\tan\alpha$ and $\tan\gamma$ as follows:

$$\begin{aligned}\left[\frac{\partial z_\xi}{\partial m_\xi}\mathcal{S}-\frac{\partial z_\xi}{\partial h_\xi}\mathcal{S}^2\right]\tan^2\gamma+\left[1-\mathcal{S}^2\right]\tan\gamma+\frac{\partial z_\xi}{\partial m_\xi}\mathcal{S}-\frac{\partial z_\xi}{\partial h_\xi} &= 0,\\ \left[\frac{\partial z_\xi}{\partial h_\xi}\mathcal{S}-\frac{\partial z_\xi}{\partial m_\xi}\mathcal{S}^2\right]\tan^2\alpha+\left[1-\mathcal{S}^2\right]\tan\alpha+\frac{\partial z_\xi}{\partial h_\xi}\mathcal{S}-\frac{\partial z_\xi}{\partial m_\xi} &= 0.\end{aligned} \tag{6}$$

Each equation has two solutions, which are:

$$\begin{aligned}-\tan\gamma &= \frac{\mathcal{S}^2-1\pm\sqrt{(1-\mathcal{S}^2)^2-4\left[\frac{\partial z_\xi}{\partial m_\xi}\mathcal{S}-\frac{\partial z_\xi}{\partial h_\xi}\mathcal{S}^2\right]\left[\frac{\partial z_\xi}{\partial m_\xi}\mathcal{S}-\frac{\partial z_\xi}{\partial h_\xi}\right]}}{2\left[\frac{\partial z_\xi}{\partial m_\xi}\mathcal{S}-\frac{\partial z_\xi}{\partial h_\xi}\mathcal{S}^2\right]},\\ -\tan\alpha &= \frac{\mathcal{S}^2-1\pm\sqrt{(1-\mathcal{S}^2)^2-4\left[\frac{\partial z_\xi}{\partial h_\xi}\mathcal{S}-\frac{\partial z_\xi}{\partial m_\xi}\mathcal{S}^2\right]\left[\frac{\partial z_\xi}{\partial h_\xi}\mathcal{S}-\frac{\partial z_\xi}{\partial m_\xi}\right]}}{2\left[\frac{\partial z_\xi}{\partial h_\xi}\mathcal{S}-\frac{\partial z_\xi}{\partial m_\xi}\mathcal{S}^2\right]}.\end{aligned} \tag{7}$$

The first of equation (7) provides the transformation from subsurface offset-domain CIG into angle-domain CIG for the converted-mode case. This theory is valid under the assumption of constant velocity. However, it remains valid in a differential sense in an arbitrary-velocity medium, by considering that h_ξ is the subsurface half offset. Therefore, the limitation of constant velocity is on the neighborhood of the image. For $\mathcal{S}(m_\xi, z_\xi)$, it is important to consider that every point of the image $I(z_\xi, m_\xi, h_\xi)$ is related to a point on the velocity model with the same coordinates.

In order to implement this equation, we observe that this can be done by an slant-stack transformation as presented on Figure 2. Note that the contribution along the midpoints is a correction factor needed in order to perform the transformation. This allows us to do the transformation from SODCIGs to ADCIGs including the lateral and vertical variations of $\mathcal{S}$.

A Fourier domain look

It is also possible to implement the transformation to full-aperture angle in the Fourier domain. Although this transformation does not take into account the lateral and vertical variations of

$\mathcal{S}$, it's still an interesting exercise. We can link this theory with Fourier transform by knowing that:

$$\frac{\partial t}{\partial m_\xi} = \frac{k_{m_\xi}}{\omega}, \quad \frac{\partial t}{\partial z_\xi} = \frac{k_{z_\xi}}{\omega}, \quad \text{and} \quad \frac{\partial t}{\partial h_\xi} = \frac{k_{h_\xi}}{\omega} \tag{8}$$

From equations (8), it is well known that

$$\frac{\partial z_\xi}{\partial h_\xi} = \frac{k_{h_\xi}}{k_{z_\xi}}, \quad \text{and} \quad \frac{\partial z_\xi}{\partial m_\xi} = \frac{k_{m_\xi}}{k_{z_\xi}}. \tag{9}$$

Therefore, the Fourier equivalent for equations (7) is

$$\begin{aligned}
-\tan\gamma &= \frac{\mathcal{S}^2 - 1 \pm \sqrt{(1-\mathcal{S}^2)^2 - 4\left[\frac{k_{m_\xi}}{k_{z_\xi}}\mathcal{S} - \frac{k_{h_\xi}}{k_{z_\xi}}\mathcal{S}^2\right]\left[\frac{k_{m_\xi}}{k_{z_\xi}}\mathcal{S} - \frac{k_{h_\xi}}{k_{z_\xi}}\right]}}{2\left[\frac{k_{m_\xi}}{k_{z_\xi}}\mathcal{S} - \frac{k_{h_\xi}}{k_{z_\xi}}\mathcal{S}^2\right]}, \\
-\tan\alpha &= \frac{\mathcal{S}^2 - 1 \pm \sqrt{(1-\mathcal{S}^2)^2 - 4\left[\frac{k_{h_\xi}}{k_{z_\xi}}\mathcal{S} - \frac{k_{m_\xi}}{k_{z_\xi}}\mathcal{S}^2\right]\left[\frac{k_{h_\xi}}{k_{z_\xi}}\mathcal{S} - \frac{k_{m_\xi}}{k_{z_\xi}}\right]}}{2\left[\frac{k_{h_\xi}}{k_{z_\xi}}\mathcal{S} - \frac{k_{m_\xi}}{k_{z_\xi}}\mathcal{S}^2\right]}.
\end{aligned} \tag{10}$$

Equations (10) can be used to transform SODCIGs into *full-aperture* ADCIGs through stretching of the offset and midpoint axes, but this is only valid for a velocity-ratio function $\mathcal{S}$ that is constant along the image ($I(z_\xi, m_\xi, h_\xi)$).

Transformation into independent angles

From equation (3) we established a relation between the propagation angles for the down-going and up-going plane-waves, β_s and β_r, respectively. Now, from Figure 1 it is easy to see that the propagation angles are related to: 1) the incidence angle of the down-going plane wave into the reflector (γ_i); 2) the reflection angle of the up-going plane wave (γ_r); and the structural dip (α_x). The relation among all the angles is

$$\beta_s = \alpha_x - \gamma_i, \quad \text{and} \quad \beta_r = \alpha_x + \gamma_r. \tag{11}$$

Combining equation (3) and (11), we can see the direct relation between the angles that we compute with relations (7) and/or (10) and the real structural dip, the incidence angle, and the reflection angle. That is:

$$\begin{aligned}
2\gamma &= \gamma_r + \gamma_i, \\
2\alpha &= 2\alpha_x + (\gamma_r - \gamma_i).
\end{aligned} \tag{12}$$

It is easy to note that the opening angle γ is the reflection angle and α is the geological dip when $\gamma_i = \gamma_r$, which is only valid for the single-mode case.

With these equations and Snell's law, we can convert the *full-aperture* angle (γ) obtained with equation (7) or (10) into the incidence angle (γ_i) or the reflection angle (γ_r):

$$\begin{aligned} \tan\gamma_i &= \frac{\phi \sin 2\gamma}{1+\phi\cos 2\gamma}, \\ \tan\gamma_r &= \frac{\sin 2\gamma}{\phi+\cos 2\gamma}. \end{aligned} \tag{13}$$

Appendix A presents a full derivation of the same equations but with the perspective of the Kirchhoff approach. The reader is encourage to follow that demonstration.

NUMERICAL ANALYSIS

First, we analyze which one of the two solutions for $\tan\gamma$ is appropriate. For this, we plot both solutions for different values of the velocity ratio ϕ. Figure 3 presents such result. The right panel presents the positive solution surface, the left panel presents the negative one. The positive solution is more stable than the negative solution. Note that the solution for the quadratic system (7) is singular when $\phi = 1$. Thus, system (7) reduces to the known relation for single-mode case. The solid blue line at $\phi = 1$ represents this case The negative solution is not well behaved for any of the values of ϕ. Figure 4 shows the first of equations (4), that is the

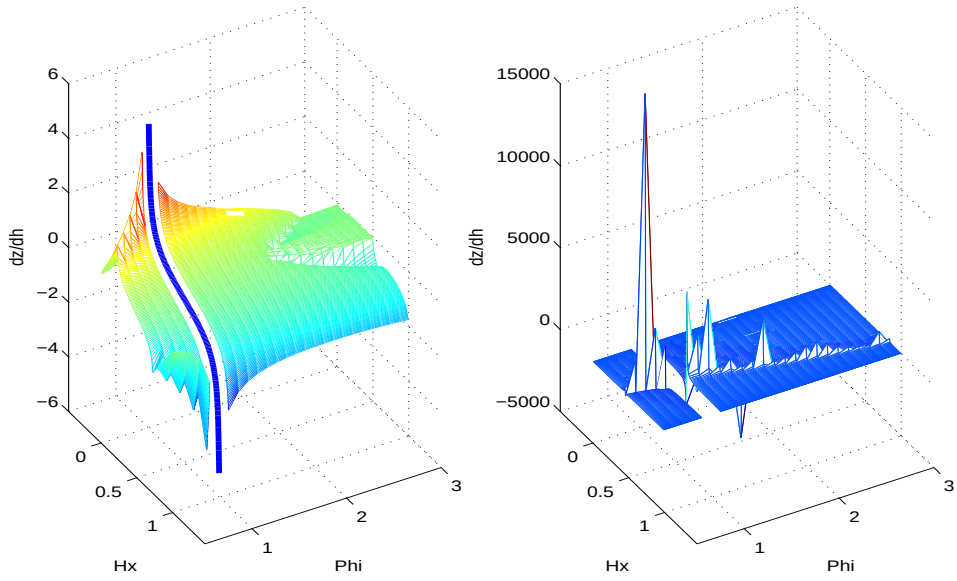

Figure 3: Both solutions for $\tan\gamma$ on equation (7). Left: Positive solution, the blue line at $\phi = 1$ corresponds to the single-mode case. Right: Negative solution. daniel2-ang_cwv_2sols [CR]

expression for the *full-aperture* angle as a function of α and the velocity ratio, ϕ. Remember that for the converted-mode case, α is related to the geologic dip (equation (12), but it's not the dip itself. In order to understand better the previous plot, we take a look at Figure 5. This figure is a cut along $\phi = 2$ on Figure 4 (dotted line) and it's compared against the conventional

approach, which is $\tan\gamma$ equals the partial derivative of depth with respect to offset. If we omit the contribution of α and ϕ, we introduce a considerable error in the transformation from SODCIGs into ADCIGs for the converted-mode case. The first of equations (4) establishes

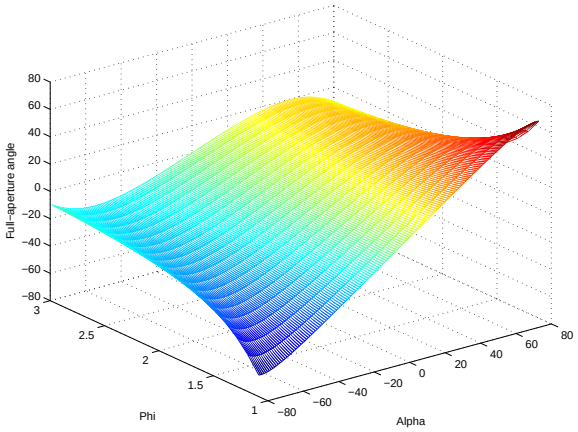

Figure 4: Full-aperture angle (γ) as a function of α and ϕ, from the first of equation (4). daniel2-ang_cwv_alpha [CR]

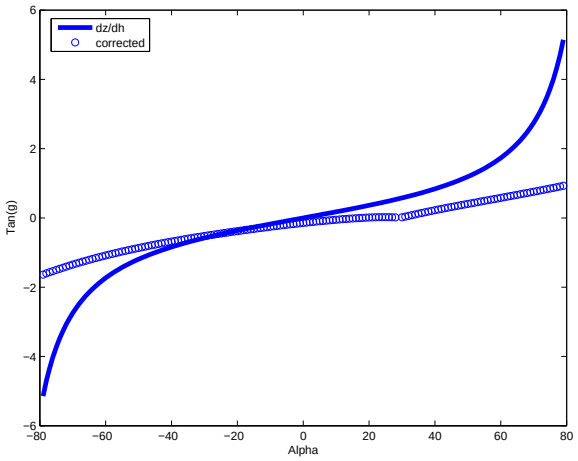

Figure 5: Difference between the conventional approach for $\tan\gamma$ (solid line) versus the transformation with the correction for α and ϕ (dotted line). This is a cut for $\phi = 2$ on Figure 4. daniel2-ang_cwv_diff [CR]

a relationship between $\tan\gamma$ and the partial derivative of depth with respect to offset. We derive this relation following a wave-equation approach. Appendix A shows that we can arrive at the same conclusion following an integral summation approach. Figure 6 summarizes both approaches. This figure presents two surfaces, both of them correspond to $\partial z/\partial h$. The color surface represents the computation with the integral summation approach (Appendix B); and the black surface represents the computation with the wave-equation approach (equation (4)). Both surfaces have a perfect match, this strongly suggests that equations (4) is accurate, and must be followed for an appropriate transformation from SODCIGs into ADCIGs for converted-mode seismic.

Synthetic model

A simple synthetic was created with constant velocity of $v_p = 2000$ and $v_s = 1000$, and varying dips. Figure 7 shows on the left the reflectivity model, and on the middle and right panels, one

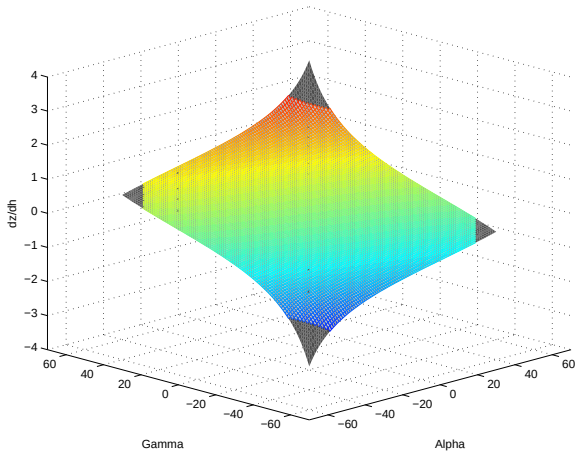

Figure 6: Wave-equation approach compared with Integral summation approach. Both of them arrive to the same surface. daniel2-ang_cwv_wei_surf_comp [CR]

single mode PP CMP gather and one converted mode PS CMP gather. The PP-CMP gather presents four reflection hyperbolas, all of them centered at zero-offset. The PS-CMP gather also presents the four reflection hyperbolas, corresponding to the same events as in the PP-CMP gather, however, they are not centered at zero-offset, as it is expected for the coverted-mode case. Also, the time axis for both synthetic data sets is different. The events on the PS CMP gather take longer to arrive, this is also a characteristic for the converted-mode case. The polarity flip is not included in this model, since it has been already discussed by Rosales and Rickett (2001b).

After wave-equation migration with the correct velocity model, the image is perfectly focused at zero subsurface offset, displayed on the left panel of Figure 8. Note, that both PP and PS sections, had the same SODCIG.

The middle and right panels of Figures 8 present the result of the transformation from SODCIGs into the single-mode ADCIG (center panel), and the the converted-mode ADCIG (right panel). It is possible to observe that the angle range (i.e. before the start of the artifacts due to the transformation in the Fourier domain) for the converted-mode ADCIG is longer than for the single-mode ADCIG, as it is expected, since the angle-information contains both the incidence and reflection angle information.

CONCLUSIONS AND FUTURE WORK

The accurate transformation from subsurface offset-domain CIGs into angle-domain CIGs for the converted-mode case requires both the information along the midpoint axis and the velocity ratio. Omitting this information yields to errors in the transformation that might transforms in wrong velocity updates. Two separate approaches to obtain the relation between the subsurface offset and the *full-aperture* angle corroborates the accuracy of our formulation.

For the converted-mode case, the angle axis of the final image ($I(z_\xi, m_\xi, \gamma)$), after the transformation, is neither the incidence nor reflection angle, but the average of both. The *full-aperture* angle gathers can be transformed into two separate angle gathers, each one represent-

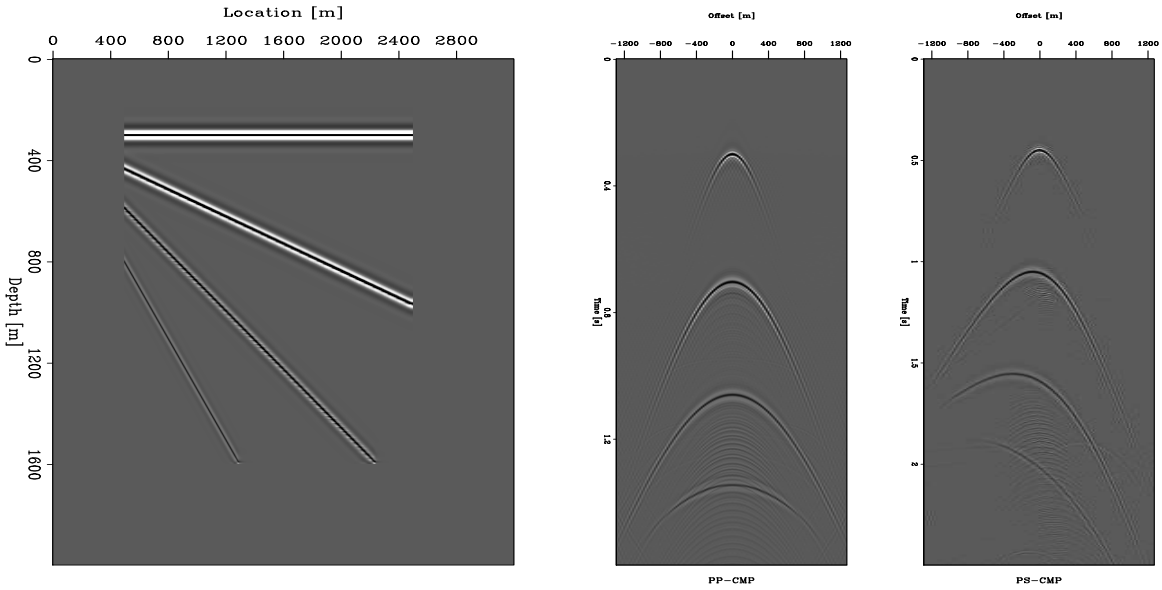

Figure 7: Synthetic data. Left: reflectivity model. Right panels: One single-mode PP CMP gather, and one converted-mode PS CMP gather. daniel2-data [CR]

ing the incidence and reflection angle. This transformations might bring useful information for the analysis of rock properties or velocity updates for the two different velocity models.

The transformation from SODCIGs into ADCIGs with a Fourier domain approach is accurate only for constant velocity. The general transformation needs to be done in the image space. Radon Transforms may provide to be a solution for this situation. The method will use the information along both the midpoint and subsurface offset axes in order to map the image into the *full-aperture* angle axis.

The next step is to analyze how errors in either P or S velocity models are transformed in the PS-ADCIGs. This will result in both a formulation for the residual moveout of converted mode data, and a methodology for vertical velocity updates of both P and S velocity models.

REFERENCES

Biondi, B., and Symes, W., 2004, Angle-domain common-image gathers for migration velocity analysis by wavefield-continuation imaging: Geophysics, **69**, no. 5, 1283–1298.

Biondi, B., 2005, Angle-domain common image gathers for anisotropic migration: SEP–**120**, 77–104.

Brandsberg-Dahl, S., de Hoop, M. V., and Ursin, B., 1999, The sensitivity transform in the common scattering-angle/azimuth domain: 61st Ann. Internat. Mtg., Soc. Expl. Geophys., Expanded Abstracts, 1538–1541.

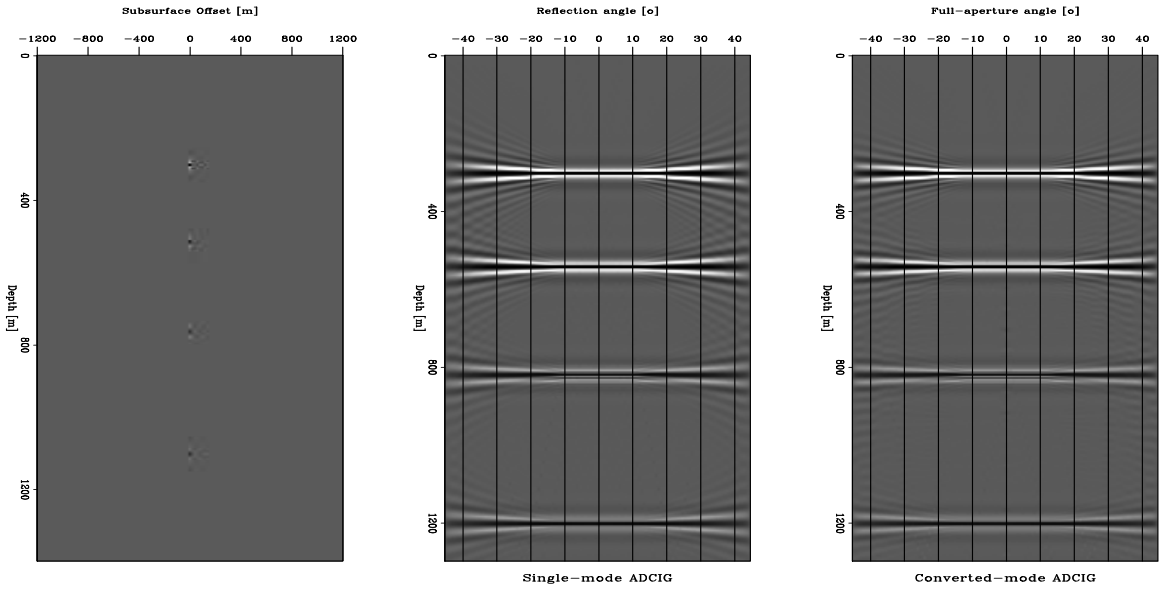

Figure 8: Subset of the image after migration. Left: one SODCIG gather. Right panels: the single-mode PP transformation to ADCIG, and the converted-mode transformation to ADCIG. daniel2-image [CR]

de Bruin, C. G. M., Wapenaar, C. P. A., and Berkhout, A. J., 1990, Angle-dependent reflectivity by means of prestack migration: Geophysics, **55**, no. 9, 1223–1234.

Fomel, S., and Prucha, M., 1999, Angle-gather time migration: SEP–**100**, 141–150.

Fomel, S., 1996, Migration and velocity analysis by velocity continuation: SEP–**92**, 159–188.

Prucha, M., Biondi, B., and Symes, W., 1999, Angle-domain common-image gathers by wave-equation migration: 69th Ann. Internat. Meeting, Soc. of Expl. Geophys., Expanded Abstracts, 824–827.

Rickett, J., and Sava, P., 2002, Offset and angle-domain common image-point gathers for shot-profile migration: Geophysics, **67**, 883–889.

Rosales, D., and Rickett, J., 2001a, ps-wave polarity reversal in angle domain common-image gathers: SEP–**108**, 35–44.

Rosales, D., and Rickett, J., 2001b, PS-wave polarity reversal in angle domain common-image gathers: 71st Annual Internat. Mtg., Expanded Abstracts, 1843–1846.

Sava, P., and Fomel, S., 2000, Angle-gathers by Fourier Transform: SEP–**103**, 119–130.

Sava, P., and Fomel, S., 2003, Angle-domain common-image gathers by wavefield continuation methods: Geophysics, **68**, no. 3, 1065–1074.

APPENDIX A

In this part, we obtain the relation to transform subsurface offset-domain common-image gathers into angle-domain common-image gathers for the case of PS data. To perform this derivation, we use the geometry in Figure 1 in order to obtain the parametric equations for migration on a constant velocity medium.

Following the derivation of Fomel (1996) and Fomel and Prucha (1999), and applying simple trigonometry and geometry to Figure A-1, we obtain parametric equations for migrating an impulse recorded at time t_D, midpoint m_D and surface offset h_D as follows:

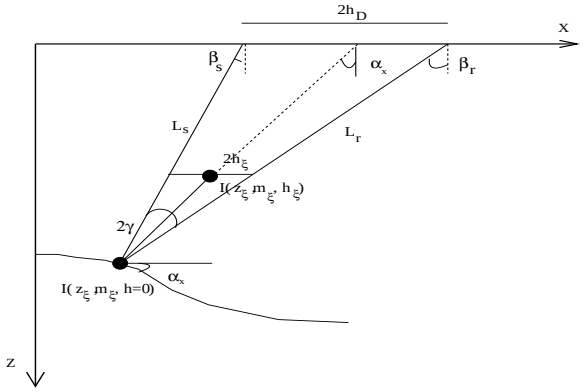

Figure A-1: Parametric formulation of the impulse response. daniel2-angles2 [NR]

$$
\begin{aligned}
z_\xi &= (L_s+L_r)\frac{\cos\beta_r\cos\beta_s}{\cos\beta_r+\cos\beta_s},\\
2h_\xi &= 2h_D+(L_s+L_r)\frac{\sin\beta_s\cos\beta_r-\sin\beta_r\cos\beta_s}{\cos\beta_r+\cos\beta_s},\\
m_\xi &= m_D-\frac{(L_s+L_r)}{2}\frac{\sin\beta_s\cos\beta_r+\sin\beta_r\cos\beta_s}{\cos\beta_r+\cos\beta_s}.
\end{aligned}
\tag{A-1}
$$

where the total path length is:

$$
\begin{aligned}
t_D &= S_sL_s+S_rL_r,\\
z_s-z_r &= L_s\cos\beta_s-L_r\cos\beta_r.
\end{aligned}
\tag{A-2}
$$

From that system of equations, Biondi (2005) shows that the total path length is

$$
L=\frac{t_D}{2}\frac{\cos\beta_r+\cos\beta_s}{S_s\cos\beta_r+S_r\cos\beta_s}.
\tag{A-3}
$$

Appendix A shows that we can rewrite system (A-1) as:

$$
\begin{aligned}
z_\xi &= \frac{(L_s+L_r)}{2}\frac{\cos^2\alpha-\sin^2\gamma}{\cos\alpha\cos\gamma},\\
2h_\xi &= 2h_D-(L_s+L_r)\frac{\sin\gamma}{\cos\alpha},\\
m_\xi &= m_D-\frac{(L_s+L_r)}{2}\frac{\sin\alpha}{\cos\gamma}.
\end{aligned}
\tag{A-4}
$$

where α and γ follow the same definition as in equation (3). where, L in terms of the angles α and β is:

$$L(\alpha,\beta) = \frac{t_D}{(S_r+S_s)+(S_r-S_s)\tan\alpha\tan\gamma} \tag{A-5}$$

Tangent to the impulse response

Following the demonstration done by Biondi (2005), the derivative of the depth with respect to the subsurface offset, at a constant image point, and the derivative of the depth with respect to the image point, at a constant subsurface offset are given by the following:

$$\left.\frac{\partial z_\xi}{\partial h_\xi}\right|_{m_\xi=\overline{m}_\xi} = -\frac{\left.\frac{\partial T}{\partial h_\xi}\right|_{m_\xi=\overline{m}_\xi}}{\left.\frac{\partial T}{\partial z_\xi}\right|_{m_\xi=\overline{m}_\xi}} = -\frac{\frac{\partial z_\xi}{\partial\alpha}\frac{\partial m_\xi}{\partial\gamma}-\frac{\partial z_\xi}{\partial\gamma}\frac{\partial m_\xi}{\partial\alpha}}{\frac{\partial m_\xi}{\partial\alpha}\frac{\partial h_\xi}{\partial\gamma}-\frac{\partial m_\xi}{\partial\gamma}\frac{\partial h_\xi}{\partial\alpha}}, \tag{A-6}$$

and

$$\left.\frac{\partial z_\xi}{\partial m_\xi}\right|_{h_\xi=\overline{h}_\xi} = -\frac{\left.\frac{\partial T}{\partial m_\xi}\right|_{h_\xi=\overline{h}_\xi}}{\left.\frac{\partial T}{\partial z_\xi}\right|_{h_\xi=\overline{h}_\xi}} = -\frac{\frac{\partial z_\xi}{\partial\gamma}\frac{\partial h_\xi}{\partial\alpha}-\frac{\partial z_\xi}{\partial\alpha}\frac{\partial h_\xi}{\partial\gamma}}{\frac{\partial m_\xi}{\partial\alpha}\frac{\partial h_\xi}{\partial\gamma}-\frac{\partial m_\xi}{\partial\gamma}\frac{\partial h_\xi}{\partial\alpha}}, \tag{A-7}$$

where the partial derivatives are:

$$\begin{aligned}
\frac{\partial z_\xi}{\partial\alpha} &= -\frac{L}{\cos\alpha\cos\gamma}\left[\tan\alpha(\cos^2\alpha+\sin^2\gamma)+\frac{(S_r-S_s)\tan\gamma(\cos^2\alpha-\sin^2\gamma)}{\cos^2\alpha}\right],\\
\frac{\partial z_\xi}{\partial\gamma} &= -\frac{L}{\cos\alpha\cos\gamma}\left[\tan\gamma(\cos^2\alpha+\sin^2\gamma)+\frac{(S_r-S_s)\tan\alpha(\cos^2\alpha-\sin^2\gamma)}{\cos^2\gamma}\right],\\
\frac{\partial m_\xi}{\partial\alpha} &= -\frac{L}{\cos\gamma}\left[\cos\alpha-\frac{(S_r-S_s)\sin\alpha\tan\gamma}{\cos^2\alpha}\right],\\
\frac{\partial m_\xi}{\partial\gamma} &= -\frac{L\sin\alpha}{\cos^2\gamma}\left[\sin\gamma-\frac{(S_r-S_s)\tan\alpha}{\cos\gamma}\right],\\
\frac{\partial h_\xi}{\partial\alpha} &= -\frac{L\sin\gamma}{\cos^2\alpha}\left[\sin\alpha-\frac{(S_r-S_s)\tan\gamma}{\cos\alpha}\right],\\
\frac{\partial h_\xi}{\partial\gamma} &= -\frac{L}{\cos\alpha}\left[\cos\gamma-\frac{(S_r-S_s)\tan\alpha\sin\gamma}{\cos^2\gamma}\right].
\end{aligned} \tag{A-8}$$

Figure A-2 presents the analytical solutions for the tangent to the impulse response. This was done for an impulse at a PS-travel time of 2 s, and a ϕ value of 2. The left panel shows the solution for equation (A-6). The right panel shows the solution for equation (A-7). The solid lines superimpose on both surfaces represents one section of the numerical derivative to the impulse response. The perfect correlation between the analytical and numerical solution validates our analytical formulations. This results supports the analysis presented with the kinematic equations.

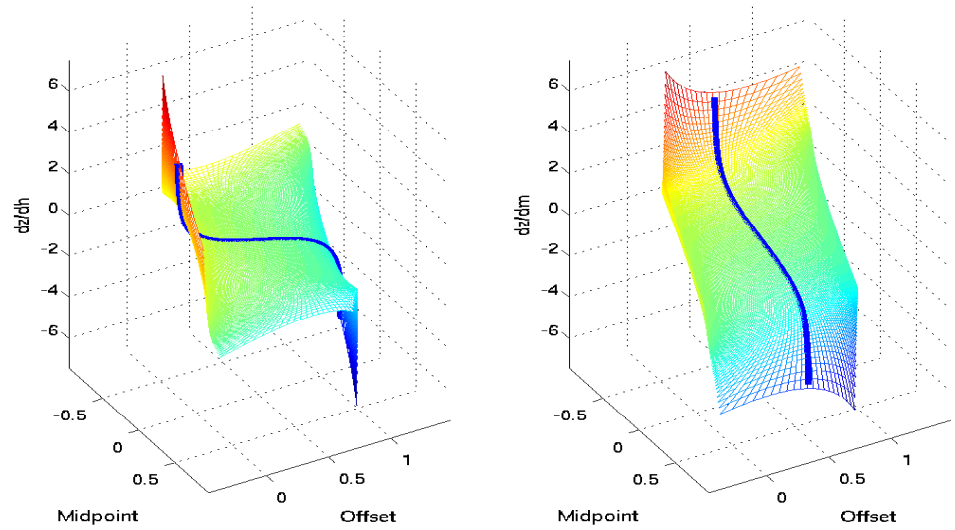

Figure A-2: Validation of the analytical solutions for the tangent to the impulse response, the surface represents the analytical solutions and superimpose is the cut with the numerical derivative. Left: For equation (A-6). Right: For equation (A-7) analytical solutions for the tangent of the spreading surface for different values of ϕ daniel2-ang_cwv_wei_surf [CR]

APPENDIX B

This section proofs the equivalence between the parametric equations A-1, that is a direct result of trigonometry and geometry on the Figure A-1, with the parametric equations A-4, which the same equations presented by previous authors.

It is important to note that even though both parametric equations A-1 and A-4 are equivalent, the difference relies on the conceptual definitions of the angles involved.

The proof of this section is pure trigonemetry, and the reader can safely skip this entire Appendix. However, this Appendix is here to show that the use of our equations is valid.

First, we rewrite β_s and β_r as function of α and γ by simple algebraic manipulation of equations 3.

$$\beta_s = \alpha - \gamma, \quad \text{and} \quad \beta_r = \alpha + \gamma. \tag{B-1}$$

The first proof is the first parametric equation:

$$\begin{aligned}
z_\xi &= (L_s+L_r)\frac{\cos\beta_r\cos\beta_s}{\cos\beta_r+\cos\beta_s}\\
&= (L_s+L_r)\frac{\cos(\alpha+\gamma)\cos(\alpha-\gamma)}{\cos(\alpha+\gamma)\cos(\alpha-\gamma)}\\
&= (L_s+L_r)\frac{(\cos\alpha\cos\gamma-\sin\alpha\sin\gamma)(\cos\alpha\cos\gamma+\sin\alpha\sin\gamma)}{2\cos\alpha\cos\gamma}\\
&= (L_s+L_r)\frac{\cos^2\alpha\cos^2\gamma-\sin^2\alpha\sin^2\gamma}{2\cos\alpha\cos\gamma}\\
&= (L_s+L_r)\frac{\cos^2\alpha\cos^2\gamma-\sin^2\gamma+\sin^2\gamma\cos^2\alpha}{2\cos\alpha\cos\gamma}\\
&= (L_s+L_r)\frac{\cos^2\alpha(\cos^2\gamma+\sin^2\gamma)-\sin^2\gamma}{2\cos\alpha\cos\gamma}\\
&= \frac{(L_s+L_r)}{2}\frac{\cos^2\alpha-\sin^2\gamma}{\cos\alpha\cos\gamma}
\end{aligned}$$

The second parametric equation is:

$$\begin{aligned}
2h_\xi &= 2h_D+(L_s+L_r)\frac{\sin\beta_s\cos\beta_r-\sin\beta_r\cos\beta_s}{\cos\beta_r+\cos\beta_s}\\
&= 2h_D+(L_s+L_r)\frac{\sin(\beta_s-\beta_r)}{2\cos\left(\frac{\beta_s+\beta_r}{2}\right)\cos\left(\frac{\beta_r-\beta_s}{2}\right)}\\
&= 2h_D+(L_s+L_r)\frac{\sin(-2\gamma)}{2\cos\alpha\cos\gamma}\\
&= 2h_D+(L_s+L_r)\frac{-2\sin\gamma\cos\gamma}{2\cos\alpha\cos\gamma}\\
&= 2h_D-(L_s+L_r)\frac{\sin\gamma}{\cos\alpha}
\end{aligned}$$

The third parametric equation is:

$$\begin{aligned}
m_\xi &= m_D-\frac{(L_s+L_r)}{2}\frac{\sin\beta_s\cos\beta_r+\sin\beta_r\cos\beta_s}{\cos\beta_r+\cos\beta_s}\\
&= m_D-\frac{(L_s+L_r)}{2}\frac{\sin(\beta_s+angr)}{2\cos\left(\frac{\beta_s+\beta_r}{2}\right)\cos\left(\frac{\beta_r-\beta_s}{2}\right)}\\
&= m_D-\frac{(L_s+L_r)}{2}\frac{\sin(2\alpha)}{2\cos\alpha\cos\gamma}\\
&= m_D-\frac{(L_s+L_r)}{2}\frac{2\sin\alpha\cos\alpha}{2\cos\alpha\cos\gamma}\\
&= m_D-\frac{(L_s+L_r)}{2}\frac{\sin\alpha}{\cos\gamma}
\end{aligned}$$